Analysis and Design of Photonic Crystal Fibers Based on an Improved Effective-Index Method

Hongbo Li, Arash Mafi, Axel Schülzgen, Li Li, Valery L. Temyanko, Nasser Peyghambarian, and Jerome V. Moloney

***Abstract*—The modal characteristics of photonic crystal fibers (PCFs), with guiding cores consisting of one or seven missing airholes, are investigated with the finite element method and compared to those of step-index fibers (SIFs). To extend the applicability of the classical SIF theories to PCFs, the effective refractive index of photonic crystal cladding and the effective core radius of a PCF are studied systematically, based on simple physically consistent concepts. With the new effective cladding index and core radius of PCFs, the classical definition of the V parameter for SIFs is extended to PCFs, and a highly efficient approach based on the effective-index method is developed for the design of PCFs. The new design approach has been successfully employed to analyze the modal properties of PCF lasers with depressed-index cores and further tested by using it to effectively estimate the number of guided modes for PCFs with large cores.**

***Index Terms*—Effective-index method (EIM), fiber laser, photonic crystal fiber (PCF), V parameter.**

I. Introduction

NUMERICAL simulations of photonic crystal fibers (PCFs) [1], [2] have confirmed that strong analogies can be drawn between the modal behavior of the PCFs and that of conventional circular step-index fibers (SIFs). In this paper, we elaborate on some of these analogies, investigate the effective refractive index of the photonic crystal cladding, the effective core radius, and the V parameter of the PCFs, and show how these results can be used to derive efficient design tools based on the effective-index method (EIM) for PCFs. Our results are particularly useful for experimentalists who would like to readily design PCFs with specific modal characteristics before studying them using a computationally expensive approach such as the finite element method (FEM). Unlike axisymmetric SIFs, there are no known analytical solutions to PCFs due to their complex structures. Hence, the analogies between the modal behaviors of the PCFs and the SIFs can be used to gain intuitive understanding of the complex modal properties of PCFs based on those of analytically solvable SIFs. For example, the endlessly single-mode behavior of PCFs, as reported initially in [3], can be explained by an effective V parameter defined analogously to that of SIFs [3]–[8]. Such quantities as the V parameter, the core and cladding refractive indexes, and the core radius in SIFs have direct analogies in PCFs and can be successfully used in the PCF design once properly defined for PCFs.

To avoid using computationally expensive numerical approaches for designing PCFs, a great deal of research has been devoted to thoroughly investigate the aforementioned analogies between the modal properties of PCFs and the classical SIFs, and various simplified approaches have been developed [3], [5], [6], [8]–[10], [12]. In general, these approaches can be categorized into the following: 1) empirical relation-based approaches [6], [8], [9] or 2) EIMs [3], [5], [10], [12]. Approaches based on empirical relations usually involve curve fitting the numerically calculated V parameters as a function of the dimensionless feature parameters d/Λ and λ/Λ of a PCF, where d, Λ, and λ are the airhole diameter, the pitch of the lattice of air holes, and the wavelength, respectively. The modal properties such as the dispersion of the PCF are then derived directly from the V parameter. These approaches have the advantage of being computationally efficient; there, however, exists a major disadvantage of having too many fitting parameters in the empirical relations (e.g., in [9, Eq. (5)]) which are difficult to recalibrate if the refractive index of the PCF glass is changed, even very slightly (e.g., by 0.01). The approaches based on the EIM consider a PCF as a special SIF with a cladding index determined by computing the effective refractive index of the photonic crystal cladding. Although the core index is well defined in the EIM, the effective core radius is not uniquely specified. In practice, different EIM-based approaches have adopted different effective core radii: fixed [3], [5], [12] or varying with d/Λ [10]. Compared with approaches based on empirical relations, the EIM-based approaches are more physically intelligible; they, however, render the computation of the effective cladding index and the specification of the effective core radius.

In this paper, we propose a computationally efficient EIM-based approach for PCFs with one or seven missing airholes by systematically studying the effective refractive index of the photonic crystal cladding and the effective core radius of the PCF. Unlike the previous EIM-based approaches, where computationally expensive numerical approaches such as FEM were used to calculate the effective cladding index, an empirical equation with only three parameters is used to efficiently and fairly accurately approximate the effective cladding index over a large parameter region of d/Λ (0.15–0.7) and λ/Λ (0.05–0.5).

Manuscript received May 24, 2006; revised January 18, 2007. This work was supported by the Air Force Office for Scientific Research, Air Force Material Command, USAF, under Grant AFOSR F49620-02-1-0380.

H. Li and J. V. Moloney are with the College of Optical Sciences and the Arizona Center for Mathematical Sciences, University of Arizona, Tucson, AZ 85721 USA (e-mail: hongbo@email.arizona.edu; jml@acms.arizona.edu).

A. Mafi is with the Corning, Inc., Corning, NY 14831 USA (e-mail: Mafi@corning.com).

A. Schülzgen, L. Li, V. L. Temyanko, and N. Peyghambarian are with the College of Optical Sciences, University of Arizona, Tucson, AZ 85721 USA (e-mail: axel@optics.arizona.edu; lli@email.arizona.edu; vtemyanko@optics.arizona.edu; nnp@u.arizona.edu).

Digital Object Identifier 10.1109/JLT.2007.893924

Another advantage of the empirical relation adopted here is that the same set of parameters can be used without recalibration if the refractive index of the photonic cladding glass is varied by a small amount (between -0.02 and $+0.02$). In previously proposed EIMs, the effective core radius was taken either as a constant specified from numerical observations or geometrical considerations [3], [5], [12] or as a function of d/Λ determined by a pure statistical approach [10]. It is addressed in [10] that a d/Λ-dependent R/Λ is physically intelligible and can greatly improve the accuracy of the EIM. In this paper, the effective core radius for PCFs with one or seven missing airholes is calculated as a function of d/Λ and λ/Λ by matching the fields of the fundamental mode in the core and the cladding. This intuitive approach is more physically intelligible and has been successfully tested and validated in this paper. Based on the new effective cladding index and core radius of the PCF, the classical definition of the V parameter for SIFs is extended to be applicable to the analysis and design of PCFs. Complex photonic crystal structures, such as depressed-index core PCFs (with one or seven missing airholes) in [11] and [12], can be easily understood and efficiently designed using the V parameter defined here. It is worth noting that this paper is focused on the PCFs made up of phosphate glass, which allows for high Er- and Yb-doping levels without detrimental clustering effects [13] and, thus, is important in fiber lasers and amplifiers. It is expected that the design concepts developed in this paper can be easily extended to other types of glass such as silica-based glass, considering the small difference between the indexes of phosphate glass and silica glass.

In Section II, an overview of PCFs with one or seven missing airholes is provided, and the effective refractive indexes of the cladding and the principal guided modes of these PCFs are computed. An empirical equation with three parameters is used to fit the effective cladding indexes as well as the effective refractive indexes of the principal guided modes. The results in Section II are used in Section III to compute the effective core radii and the V parameters of the corresponding PCFs. In Section IV, the EIM-based design approach is employed to analyze the modal properties of the PCF lasers with depressed-index cores [12]. The approach is further tested by using it to estimate the number of guided modes in the PCF lasers.

II. Cladding and Modal Refractive Indexes

The PCFs considered in this paper are optical fibers with a triangular lattice of airholes in the cladding region. The airholes have a diameter d and run through the full length of the optical fiber [1], [2]. One or several missing airholes in the center of a PCF constitute a defect in the lattice (Fig. 1), acting as a guiding core for the propagating modes in the PCF through a mechanism similar to the total internal reflection in SIFs [3]. The presence of airholes in the cladding region lowers the effective refractive index of the cladding $n_{\rm cl}$ below the refractive index of the core $n_{\rm co}$, and an effective index step is created between the core and the cladding regions. Unlike SIFs, the effective refractive index of the cladding $n_{\rm cl}$ of a PCF is determined by the amount of overlap between the fundamental space-filling mode (FSM) and the glass material

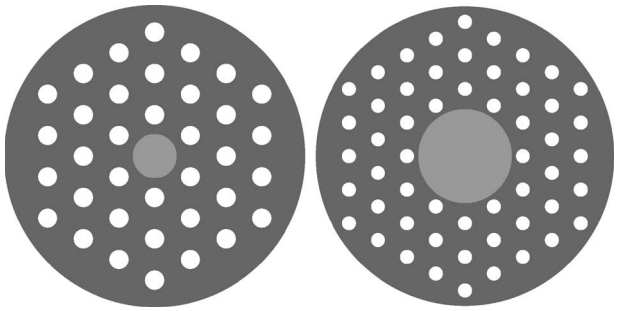

Fig. 1. PCFs with one or seven missing airholes. The cores are marked for illustration purpose only.

in the cladding and, thus, is a strong function of parameters λ, Λ, and d. In fact, the scale invariance of Maxwell equations implies that any physical quantity that characterizes a PCF and its guided modes must be a function of the dimensionless feature parameters d/Λ and λ/Λ. The complex behavior of $n_{\rm cl}$ as a function of the feature parameters is responsible for such exotic phenomena as endlessly single-mode behavior [3], large-mode-area PCFs [14], and highly nonlinear PCFs with unique dispersion properties [15]–[17].

A great deal of effort has been devoted to the calculation of $n_{\rm cl}$ as a function of the PCF feature parameters by semianalytical or numerical methods. It was observed in [3] that $n_{\rm cl}$ can be evaluated as the effective refractive index of the principal mode (with the largest propagation constant) of the PCF without defects, which is often referred to as the FSM. To calculate $n_{\rm cl}$, Birks *et al.* [3] solve the scalar Helmholtz equation over the unit hexagonal cell of the photonic crystal cladding, with the Neumann boundary condition (BC) imposed on the edges based on the reflection symmetry. The hexagonal cell is then approximated with a circular cell whose circular symmetry allows for an analytical solution, from which the FSM and $n_{\rm cl}$ are calculated. There are a few studies that use vectorial methods to calculate the FSM and its refractive index $n_{\rm cl}$. For example, Midrio *et al.* [19] find an analytical solution similar to the one in [3] but in a vectorial form. The BCs on the circular cell with which the hexagonal unit cell is approximated are perfectly electric (PE) and perfectly magnetic (PM), derived from symmetry arguments. The radius of the circle is undetermined in this model, and numerical simulations were conducted to justify the choice of $\Lambda/2$ as the radius. Another vectorial approach discussed in [18] makes use of the fact that the defect-free PCF is a periodic structure where the magnetic field and the background dielectric constant can be expanded in discrete Fourier series. The expansion coefficients of the dielectric constant are calculated analytically, and the expansion coefficients of the magnetic field are solved as an eigenvalue problem in a matrix equation. The number of Fourier modes (plane waves) determines the size of the matrix and, consequently, the accuracy of the method. In this paper, we adopt a different method that is based on a vectorial finite element analysis introduced in [7]. It is worth noting that the results of the vectorial methods indicate that the scalar approximation is not adequate for calculating $n_{\rm cl}$, especially when d/Λ and/or λ/Λ are large.

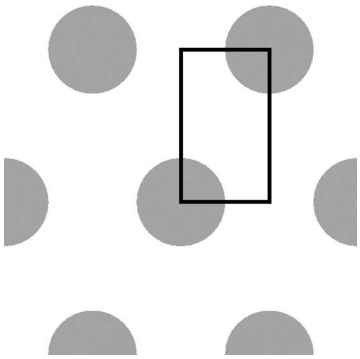

Fig. 2. Rectangular region over which the effective refractive index of the photonic crystal cladding is calculated.

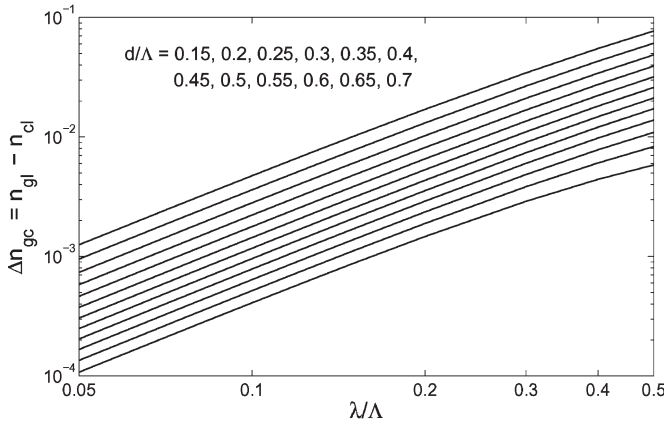

Fig. 3. $\Delta n_{\rm gc}$ as a function of λ/Λ for fixed d/Λ. Adjacent lines are in increments of $d/\Lambda = 0.05$. The lowest line corresponds to $d/\Lambda = 0.15$ and the highest to $d/\Lambda = 0.7$.

The elementary region [7] as shown in Fig. 2 is used in the vectorial finite element analysis to calculate $n_{\rm cl}$. With appropriate BCs [7], [19] applied on the edges of the rectangular region in Fig. 2, the eigenmode with the largest propagation constant is solved for the rectangular unit cell. A PE BC on the longer sides and PM on the shorter sides of the rectangular region or vice versa yield both polarizations of the FSM. The two polarization-degenerate FSMs resemble two polarizations of a plane wave in the limit of $\omega \to 0$. A refractive index of $n_{\rm gl} = 1.56$, which is typical for phosphate glass, is chosen as the default value in the simulations in this paper. The numerical studies are performed mainly over a parameter region of d/Λ (0.15–0.7) and λ/Λ (0.05–0.5), where there are a variety of applications such as PCF lasers [11], [12].

The computed $\Delta n_{\rm gc}$ (i.e., $\Delta n_{\rm gc} = n_{\rm gl} - n_{\rm cl}$, where $n_{\rm gl}$ is the refractive index of the cladding glass) is plotted in Fig. 3 as a function of λ/Λ for a set of values of d/Λ on a log-log scale. The parallel straight lines in Fig. 3 indicate that a power-law relationship exists between $\Delta n_{\rm gc}$ and λ/Λ, where the power is independent of d/Λ. An expression of the form

$$\ln \Delta n_{\rm gc} = c_1 \ln\left(\frac{\lambda}{\Lambda}\right) + c_2 \frac{d}{\Lambda} + c_3 \qquad (1)$$

with parameters c_1, c_2, and c_3 is adopted to fit the data in Fig. 3. The parameters are determined using a curve-fitting scheme

TABLE I
FITTING PARAMETERS IN (1)

Parameter	Δn_{gc}	Δn_{gm} 1 hole missing	Δn_{gm} 7 hole missing
c_1	1.87292	1.93153	1.95949
c_2	4.25125	1.95909	1.18251
c_3	-4.11279	-3.87727	-4.71681

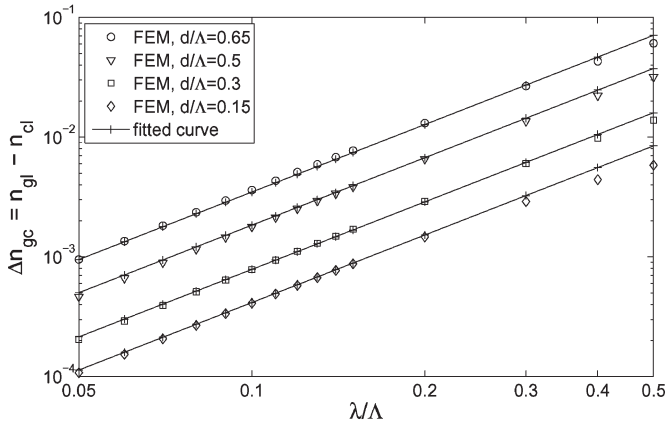

Fig. 4. Comparison of $\Delta n_{\rm gc}$ versus λ/Λ. The fitted curves are calculated using (1).

and listed in Table I. In Fig. 4, the data of $\Delta n_{\rm gc}$ in Fig. 3 are compared to those approximated with the empirical expression of (1) for a few values of d/Λ. As shown in Fig. 4, except for data points with small d/Λ and large λ/Λ, an overall good agreement is observed in the entire parameter region, indicating that (1) is an adequate approximation for the effective cladding index in the region studied.

Due to the fact that the refractive index of phosphate glass is dependent on its composition and usually deviates from the value of 1.56 used in this paper, the variation of $\Delta n_{\rm gc}$ with $n_{\rm gl}$ is investigated with $n_{\rm gl} = 1.56 \pm 0.02$. Over the entire parameter region, the relative error in $\Delta n_{\rm gc}$ caused by the variation of $n_{\rm gl}$ is found to be less than 1.8%. Hence, if the actual refractive index $n_{\rm gl}$ of the cladding glass is between 1.54 and 1.58, the effective cladding index $n_{\rm cl}$ can still be approximated with $n_{\rm cl} = n_{\rm gl} - \Delta n_{\rm gc}$, where $n_{\rm gc}$ is the same as in Fig. 3 or can be approximated with (1) without recalculating the parameters.

The modal refractive indexes $n_{\rm mo}$ of the principal modes of PCFs with one and seven missing airholes are presented as $\Delta n_{\rm gm} = n_{\rm gl} - n_{\rm mo}$ in Figs. 5 and 6, respectively, and will be used in the next section. Our fully vectorial FEM models for the PCF structures have four layers of airholes [12] surrounding the core area and are analyzed to find the principal modes and corresponding propagation constants. The effect of additional layers of airholes is found to be negligible on the value of the propagation constant, largely due to the fact that the fundamental mode is mainly concentrated in the core area and decays exponentially into the cladding region. For the PCF structures considered in this paper, the model index change $\Delta n_{\rm gm}$ shows a linear dependence on λ/Λ on a log-log scale as well and can be approximated with (1) (with $\Delta n_{\rm gm}$ in place of $\Delta n_{\rm gc}$). The corresponding fitting parameters are listed in Table I as well.

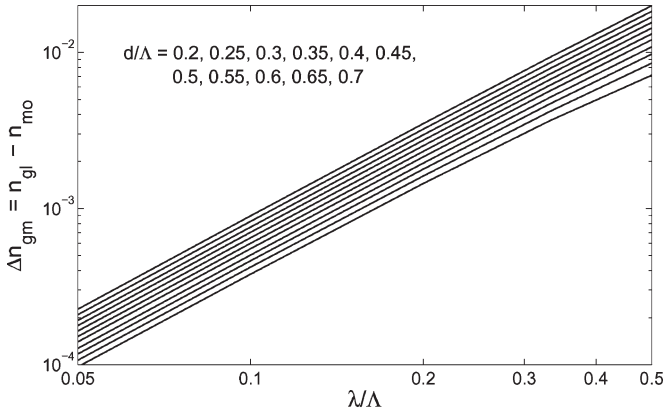

Fig. 5. $\Delta n_{\rm gm}$ as a function of λ/Λ for a PCF with a single missing airhole. Lines are in increments of $d/\Lambda = 0.05$. The lowest line corresponds to $d/\Lambda = 0.2$ and the highest to $d/\Lambda = 0.7$.

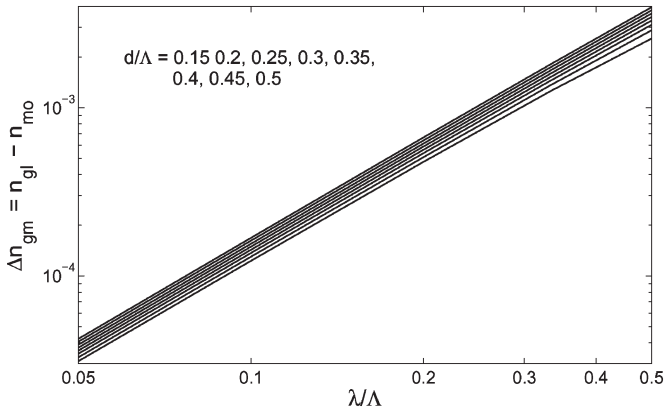

Fig. 6. $\Delta n_{\rm gm}$ as a function of λ/Λ for a PCF with seven missing airholes. Lines are in increments of $d/\Lambda = 0.05$. The lowest line corresponds to $d/\Lambda = 0.15$ and the highest to $d/\Lambda = 0.5$.

III. Effective Core Radius and the V Parameter

The modal properties of a circular SIF can be characterized by the V parameter defined as follows:

$$V = \frac{2\pi}{\lambda} R \sqrt{n_{\rm co}^2 - n_{\rm cl}^2} \tag{2}$$

where $n_{\rm co}$ and $n_{\rm cl}$ are the refractive indexes of the core and the cladding, respectively, and R is the radius of the core. The value of $V^* = 2.405$ is the single-mode cutoff for circular SIFs, above which higher order modes are supported in the fibers. A similar definition of the V parameter for PCFs was first adopted in [3] and later expanded in [5] and [6]. The studies in [3] and [5] consider Λ as the appropriate length scale to replace R in (2), while the study in [6] uses $\Lambda/\sqrt{3}$. There are also differences in the definition of $n_{\rm co}$ among these references. While the studies in [3] and [6] define $n_{\rm co}$ as the refractive index of the glass in PCF, the study in [5] assumes that $n_{\rm co}$ is the effective refractive index of the guided principal mode $n_{\rm mo} = \beta/k_0$, where β is the propagation constant, and k_0 is the wavenumber of the confined light in a vacuum. Nonetheless, there is a common definition of the refractive index of the cladding $n_{\rm cl}$ as the effective refractive index of the FSM in an infinitely extended PCF without any defect. Although all these definitions are shown to be capable of properly describing the modal behavior of PCFs for at least the simplest cases, they result in different values of the single-mode cutoff V^*. For example, V^* holds the value of π in [5], while in [6], the classical value of 2.405 is obtained. Koshiba and Saitoh [6] argue that the definition adopted in [5] is intrinsically different from (2) and actually corresponds to the normalized transverse attenuation constant in the cladding region or the W number. The U and W numbers of a circular SIF are given by

$$U = \frac{2\pi}{\lambda} R \sqrt{n_{\rm co}^2 - n_{\rm mo}^2} \tag{3}$$

$$W = \frac{2\pi}{\lambda} R \sqrt{n_{\rm mo}^2 - n_{\rm cl}^2} \tag{4}$$

where

$$V^2 = U^2 + W^2. \tag{5}$$

The choice of $\Lambda/\sqrt{3}$ in [6] as the effective core radius of PCF is justified by the numerical observations in [7]. There is also an intuitive explanation for why the effective core radius is close to $\Lambda/\sqrt{3}$. As initially reported in [3], the fundamental unit cell in a PCF with no defect is a hexagon with an edge-to-edge distance of Λ and has an airhole in its center. The core of the PCF with a single missing airhole is approximated by the central solid hexagonal cell. Since $\Lambda/\sqrt{3}$ is the center-to-corner distance in the hexagon that constitutes the core, the selection of $\Lambda/\sqrt{3}$ as the core radius by the study in [6] appears to be reasonable. However, one might argue that a more suitable parameter would be the effective radius of an equivalent circle whose area is the same as the hexagon, resulting in a value of $(\sqrt{3}/2\pi)^{1/2}\Lambda$ that is close to $\Lambda/\sqrt{3}$. Instead of using a fixed R/Λ for the effective core radius for PCFs (as in [3], [5], and [6]), Park and Lee [10] show that a d/Λ-dependent R/Λ is physically intelligible and can greatly improve the accuracy of the EIM initially proposed in [3]. In [10], a statistical approach is employed to determine R/Λ as a function of d/Λ for PCFs with a single missing airhole.

In this paper, the idea in [10] is generalized and extended to PCFs with seven missing airholes. The effective core radius R for a PCF with one or seven missing airholes is determined by solving for the scalar modal field of a circular SIF equivalent to the PCF and matching the BCs. For a PCF with the given d/Λ and λ/Λ, the equivalent SIF has a radius of R, a core refractive index $n_{\rm gl}$, and a cladding refractive index of $n_{\rm cl}$ (in Fig. 3). The scalar approximation is valid as long as the index step is low and λ/Λ is small. As shown in the previous section, the refractive index of the PCF cladding is only slightly smaller than that of the core ($n_{\rm gl}$), which justifies the use of scalar approximation in determining the effective core radius of a PCF. In the scalar approximation, the fundamental mode in the core and the cladding of the equivalent SIF is of the forms of the zeroth-order Bessel function of the first type J_0 and the zeroth-order modified Bessel function of the second type K_0, respectively. A characteristic equation is derived from the continuity of the scalar field and its first derivative

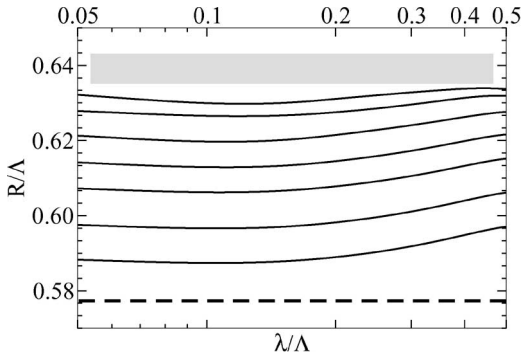

Fig. 7. Core radius of a PCF with a single missing airhole. The dashed line is for $R = \Lambda/\sqrt{3}$. Lines are in decrements of $d/\Lambda = 0.05$. Lowest corresponds to $d/\Lambda = 0.7$ and highest to $d/\Lambda = 0.4$. The gray area corresponds to $d/\Lambda < 0.4$.

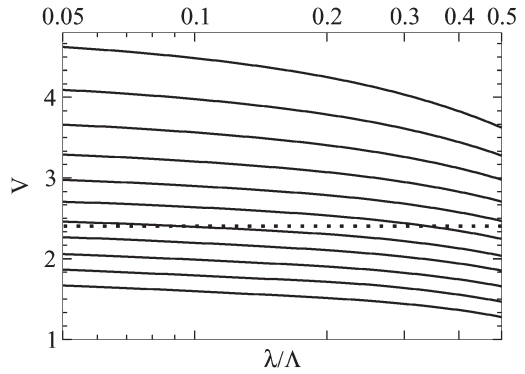

Fig. 8. V parameter of a PCF with a single missing airhole. Lines are in increments of $d/\Lambda = 0.05$. Lowest corresponds to $d/\Lambda = 0.2$ and highest to $d/\Lambda = 0.7$.

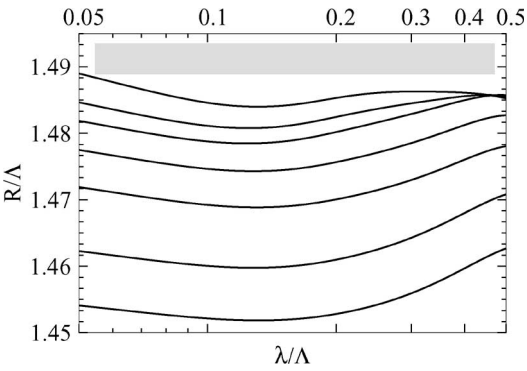

Fig. 9. Core radius of a PCF with seven missing airholes. Lines are in decrements of $d/\Lambda = 0.05$. Lowest corresponds to $d/\Lambda = 0.5$ and highest to $d/\Lambda = 0.2$. The gray area corresponds to $d/\Lambda < 0.2$.

at the boundary between the core and the cladding and is expressed as

$$\frac{J_0(U)}{UJ_1(U)} - \frac{K_0(W)}{WK_1(W)} = 0. \tag{6}$$

Since the modal refractive indexes n_{mo} of the fundamental modes of the PCFs with one and seven missing airholes are available in Figs. 5 and 6, respectively, for the given d/Λ and λ/Λ, U and W [in (3) and (4)] are only dependent on R. Therefore, R can be solved from (6) as a function of d/Λ and λ/Λ. The corresponding V parameter can be computed

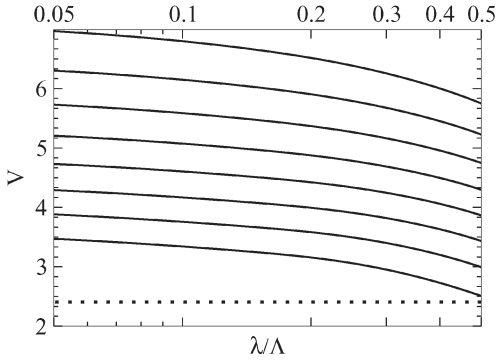

Fig. 10. V parameter of a PCF with seven missing airholes. Lines are in increments of $d/\Lambda = 0.05$. Lowest corresponds to $d/\Lambda = 0.15$ and highest to $d/\Lambda = 0.5$.

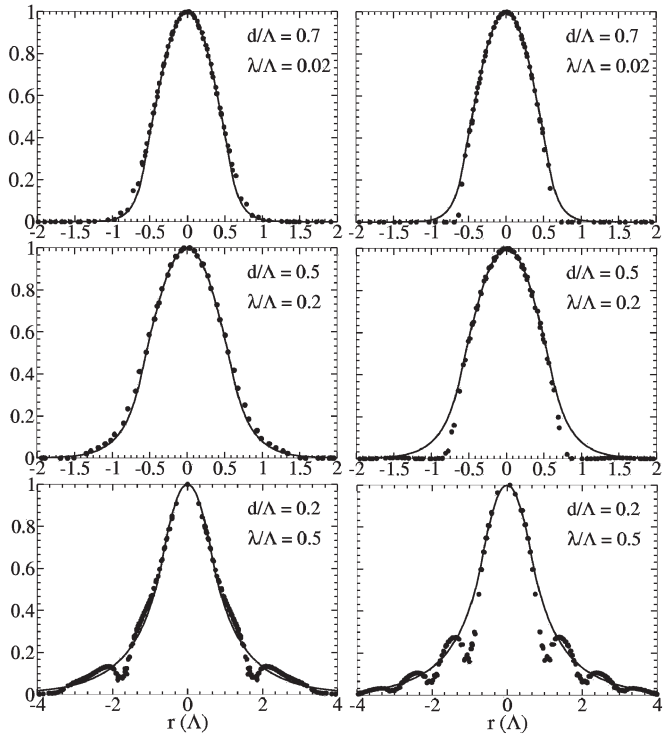

Fig. 11. Transverse profile of the principal mode of a PCF from FEM (dots) plotted against the Bessel functions from (6) (solid line) in different directions. The analyzed PCF has a single missing airhole in the center.

from (2). It is worth nothing that in (2), both R and n_{cl} are dependent on the dimensionless feature parameters d/Λ and λ/Λ. The effective core radius and the V parameter for PCFs with a single missing airhole are plotted in Figs. 7 and 8; those for PCFs with seven missing airholes are plotted in Figs. 9 and 10. To justify the use of (6) to calculate the effective core radius R, we compute the principal mode of a PCF with a single missing airhole, as shown in Fig. 1, and compare the numerical results with the analytical solution of the principal mode of the equivalent SIF. In Fig. 11, the plots in the left column correspond to the modal profiles along the horizontal line going through the center of the PCF, while the plots in the right column are the modal profiles along a line through the center and at an angle of 30° relative to the horizontal direction. The dotted lines are from the FEM simulations, while the

continuous lines are from analytical solutions. The first row is for $d/\Lambda = 0.7$ and $\lambda/\Lambda = 0.02$, where a very good agreement between the FEM results and our analytical approximations is expected. The second row corresponds to $d/\Lambda = 0.5$ and $\lambda/\Lambda = 0.2$, where moderate agreement is expected, and the third row is for $d/\Lambda = 0.2$ and $\lambda/\Lambda = 0.5$ where we expect to see the least amount of agreement. A fairly good agreement is observed in all three cases in Fig. 11, indicating that our approximations are holding well in the entire parameter region studied in this paper. Deviations in the right column of Fig. 11 are due to the presence of the airholes in the lattice structure, yet the overall envelope of the field is properly predicted by (6).

IV. Validation of the Design Approach

The design approach based on the concepts of the effective cladding index, the effective core radius, and the classical definition of the V parameter (2) for PCFs is employed to investigate the modal properties of PCF lasers (MOF7s) in [12], which have depressed-index cores formed by seven missing airholes in the center. The MOF7s have a 125-μm outer diameter and a 9-μm pitch (Λ). The lasing wavelength is around 1.535 μm and is fixed. The refractive index of the photonic crystal cladding glass $n_{\rm gl}$ is 1.569, while the index of the active core $n_{\rm co}$ is depressed by $\Delta n_d = n_{\rm co} - n_{\rm gl}$. The experimental data on MOF7s with $\Delta n_d = -7 \times 10^{-4}$ and -15×10^{-4} are investigated here. In the experiment, MOF7s with different airhole diameters d are tested, and the measured modal qualities (M^2 values) versus d/Λ are shown in [12, Fig. 2]. It is concluded in [12] that for MOF7s with $\Delta n_d = -7 \times 10^{-4}$, the PCF laser with d/Λ of 0.2 (and a standard deviation of 0.025) is in the single-mode region. To test our design approach, the V parameter defined in (2) is redefined as

$$V = \frac{2\pi}{\lambda} R \sqrt{(n_{\rm gl} + \Delta n_d)^2 - (n_{\rm gl} - \Delta n_{\rm gc})^2} \qquad (7)$$

for MOF7s with depressed-index core and is recalculated. It is worth noting that in [12], a constant value is adopted for the effective core radius R, and the vectorial FEM is employed to calculate the effective refractive index of the PCF cladding. With the new design approach, R is set to be dependent on d/Λ and λ/Λ, and (1) is employed to determine the effective cladding index $n_{\rm cl}$ with good accuracy. Fig. 12 shows the calculated V parameter as a function of d/Λ for $\Delta n_d = -7 \times 10^{-4}$ and -15×10^{-4}. Adapting the single-mode cutoff of $V^* = 2.405$ for circular SIFs, a single-mode region of d/Λ less than 0.188 is observed for $\Delta n_d = -7 \times 10^{-4}$ in Fig. 12. This is consistent with the corresponding experimental data, where the single-mode operation was obtained for MOF7s with $d/\Lambda < 0.2$ and a standard deviation of 0.025 in d/Λ. For $\Delta n_d = -15 \times 10^{-4}$, a single-mode cutoff occurs at d/Λ around 0.29, which agrees with the experimental observation of the single-mode operation of the MOF7 with $d/\Lambda = 0.264$. For $\Delta n_d = -15 \times 10^{-4}$ in Fig. 12, when d/Λ becomes so small that $n_{\rm cl}$ is greater than $n_{\rm co}$, the V parameter becomes zero (the real part of a purely imaginary number), and no core confined mode will be supported in the PCF. This is analogous to index antiguiding in SIFs. The simulation results are consistent with the experiment

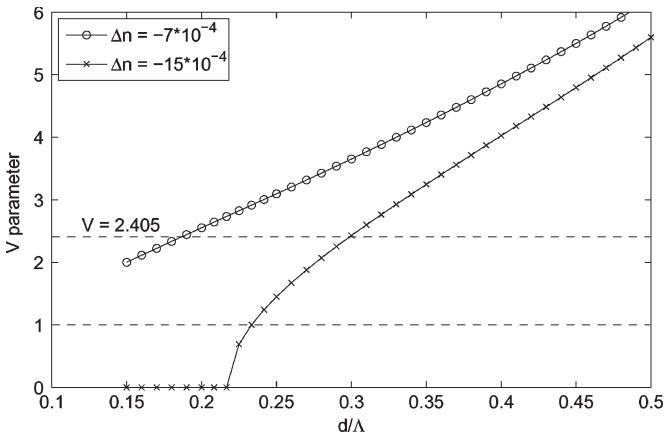

Fig. 12. V parameter versus d/Λ for MOF7s with depressed-index cores. The light wavelength λ and lattice pitch Λ are fixed.

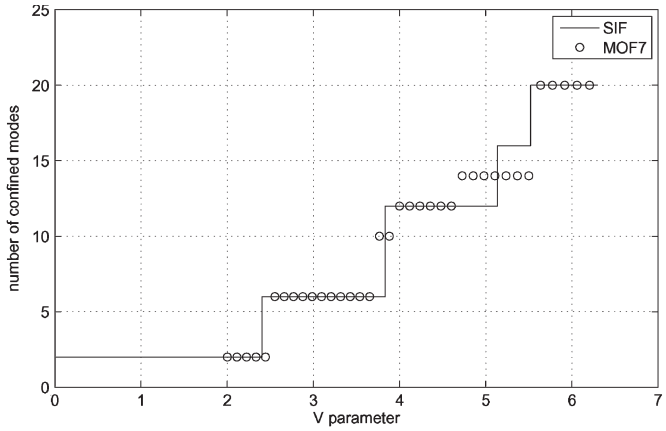

Fig. 13. Number of confined modes versus V parameter for MOF7s. The solid line represents the predicted results using the V parameter of MOF7 and the SIF theory, while the open circles are obtained with FEM simulation.

data, where M^2 increases rapidly as d/Λ decreases below 0.25, indicating that the MOF7s approach index antiguiding.

As mentioned above, the modal properties of an SIF is characterized by the V parameter. To further validate the new design approach for PCFs, it is important to compare the number of confined modes predicted by the V parameter of a PCF and that obtained from the FEM simulation. The MOF7s with both $\Delta n_d = 0$ and $\Delta n_d = -7 \times 10^{-4}$ are used here as an example and analyzed with the vectorial FEM to yield the relation between the number of confined modes and d/Λ. The relation between the number of confined modes and the V parameter is then obtained since d/Λ has a one-to-one correspondence with the V parameter (e.g., the one-to-one correspondence between the V parameter and d/Λ for $\Delta n_d = -7 \times 10^{-4}$ in Fig. 12). Since the relations between the number of confined mode and the V parameter are almost identical for both values of Δn_d, only the results for $\Delta n_d = -7 \times 10^{-4}$ are presented and shown in Fig. 13. The solid line in Fig. 13 is obtained from the SIF theory, where the polarization degeneracy of the confined modes is taken into account. For example, in a single-mode SIF, there are two linearly independent $\rm HE_{11}$ modes that can be resolved by FEM simulations. In Fig. 13, it can be observed that an overall fair agreement between the results of the finite element simulation and those of the V parameter-based design

procedure is achieved. For the MOF7 with $d/\Lambda = 0.5$, the corresponding V parameter is 6.205, indicating that there are 20 confined modes supported in the MOF7. From the SIF theory, the 20 modes are $HE_{11}(2)$ (with "2" denoting twofold polarization degeneracy), $TE_{01}(1)$, $TM_{01}(1)$, $HE_{21}(2)$, $HE_{12}(2)$, $EH_{11}(2)$, $HE_{31}(2)$, $EH_{21}(2)$, $HE_{41}(2)$, $TE_{02}(1)$, $TM_{02}(1)$, and $HE_{22}(2)$. The FEM simulation of the same MOF7 yields the same number of confined modes; furthermore, each mode from the FEM simulation closely resembles one of the 20 modes of the SIF with the same V parameter. It is worth noting that since an MOF7 has a lower order of rotational symmetry than its equivalent SIF, the cutoff values of higher order modes for the MOF7 deviate from those of its equivalent SIF, leading to the difference in the number of modes when the V parameter is around five, as shown in Fig. 13. Encouragingly, the number of confined modes estimated by the V parameter is consistent with that from the FEM simulations as the V parameter increases.

V. Conclusion

In this paper, the modal properties of PCFs with guiding cores consisting of one or seven missing airholes are comprehensively investigated. Based on the analogies between SIFs and PCFs, the concepts of the effective refractive index of photonic crystal cladding and the effective core radius are systematically studied and reformulated for PCFs. With the new effective cladding index and the effective core radius, the classical SIF theories, including the V parameter, are extended to be applicable to the analysis and design of PCFs. The new design approach is validated by using it in properly characterizing the modal properties of the PCF lasers with depressed-index cores and effectively estimating the number of core-confined modes for PCFs. This EIM-based approach can be used as a simple and efficient tool for experimentalists to design PCFs with specific modal properties.

References

[1] J. C. Knight, T. A. Birks, P. S. J. Russell, and D. M. Atkin, "All-silica single-mode optical fiber with photonic crystal cladding," *Opt. Lett.*, vol. 21, no. 19, pp. 1547–1549, Oct. 1996.

[2] J. C. Knight, T. A. Birks, P. S. J. Russell, and D. M. Atkin, "All-silica single-mode optical fiber with photonic crystal cladding: Errata," *Opt. Lett.*, vol. 22, no. 7, pp. 484–485, Apr. 1997.

[3] T. A. Birks, J. C. Knight, and P. S. J. Russell, "Endlessly single-mode photonic crystal fiber," *Opt. Lett.*, vol. 22, no. 13, pp. 961–963, Jul. 1997.

[4] B. T. Kuhlmey, R. C. McPhedran, and C. M. de Sterke, "Modal cutoff in microstructured optical fibers," *Opt. Lett.*, vol. 27, no. 19, pp. 1684–1686, Oct. 2002.

[5] N. A. Mortensen, J. R. Folkenberg, M. D. Nielsen, and K. P. Hansen, "Modal cutoff and the V parameter in photonic crystal fibers," *Opt. Lett.*, vol. 28, no. 20, pp. 1879–1881, Oct. 2003.

[6] M. Koshiba and K. Saitoh, "Applicability of classical optical fiber theories to holey fibers," *Opt. Lett.*, vol. 29, no. 15, pp. 1739–1741, Aug. 2004.

[7] F. Brechet, J. Marcou, D. Pagnoux, and P. Roy, "Complete analysis of the characteristics of propagation into photonic crystal fibers, by the finite element method," *Opt. Fiber Technol.*, vol. 6, no. 2, pp. 181–191, Apr. 2000.

[8] M. D. Nielsen and N. A. Mortensen, "Photonic crystal fiber design based on the V parameter," *Opt. Express*, vol. 11, no. 21, pp. 2762–2768, Oct. 2003.

[9] K. Saitoh and M. Koshiba, "Empirical relations for simple design of photonic crystal fibers," *Opt. Express*, vol. 13, no. 1, pp. 267–274, Jan. 2005.

[10] K. N. Park and K. S. Lee, "Improved effective-index method for analysis of photonic crystal fibers," *Opt. Lett.*, vol. 30, no. 9, pp. 958–960, May 2005.

[11] L. Li, A. Schülzgen, V. L. Temyanko, T. Qiu, M. M. Morrell, Q. Wang, A. Mafi, J. V. Moloney, and N. Peyghambarian, "Short-length microstructured phosphate glass fiber lasers with large mode areas," *Opt. Lett.*, vol. 30, no. 10, pp. 1141–1143, May 2005.

[12] L. Li, A. Schülzgen, V. L. Temyanko, H. Li, S. Sabet, M. M. Morrell, A. Mafi, J. V. Moloney, and N. Peyghambarian, "Investigation of modal properties of microstructured optical fibers with large depressed-index cores," *Opt. Lett.*, vol. 30, no. 24, pp. 3275–3277, Dec. 2005.

[13] S. Jiang, S. Mendes, Y. Hu, G. Nunzi-Conti, A. Chavez-Pirson, Y. Kaneda, T. Luo, S. Hocde, D. T. Nguyen, E. Wright, J. Wang, W. Tian, T. Nikolajsen, and N. Peyghambarian, "Compact multimode pumped erbium-doped phosphate fiber amplifiers," *Opt. Eng.*, vol. 42, no. 10, pp. 2817–2820, Oct. 2003.

[14] J. C. Knight, T. A. Birks, R. F. Cregan, P. S. J. Russell, and J.-P. De Sandro, "Large mode area photonic crystal fibre," *Electron. Lett.*, vol. 34, no. 13, pp. 1347–1348, Jun. 1998.

[15] D. Mogilevtsev, T. A. Birks, and P. S. J. Russell, "Group-velocity dispersion in photonic crystal fibers," *Opt. Lett.*, vol. 23, no. 21, pp. 1662–1664, Nov. 1998.

[16] A. Ferrando, E. Silvestre, J. J. Miret, and P. Andrs, "Nearly zero ultraflattened dispersion in photonic crystal fibers," *Opt. Lett.*, vol. 25, no. 11, pp. 790–792, Jun. 2000.

[17] J. C. Knight, J. Arriaga, T. A. Birks, A. Ortigosa-Blanch, W. J. Wadsworth, and P. S. J. Russell, "Anomalous dispersion in photonic crystal fiber," *IEEE Photon. Technol. Lett.*, vol. 12, no. 7, pp. 807–809, Jul. 2000.

[18] Z. Zhu and T. G. Brown, "Analysis of the space filling modes of photonic crystal fibers," *Opt. Express*, vol. 8, no. 10, pp. 547–554, May 2001.

[19] M. Midrio, M. P. Singh, and C. G. Someda, "The space filling mode of holey fibers: An analytical vectorial solution," *J. Lightw. Technol.*, vol. 18, no. 7, pp. 1031–1037, Jul. 2000.

Hongbo Li received the M.Sc. degree in optical sciences from the University of Arizona, Tucson, in 2006, where he is currently working toward the Ph.D. degree at the College of Optical Sciences.

His current research interests include numerical modeling of fiber lasers and semiconductor lasers.

Arash Mafi received the Ph.D. degree from The Ohio State University, Columbus, in 2001.

From 2001 to 2002, he was a Research Associate with the Physics Department, University of Arizona, Tucson, where he worked on the phenomenology of superstrings and supersymmetric grand unified theories with extra dimensions. He then joined the Optical Sciences Center and Arizona Center for Mathematical Sciences, University of Arizona, as a Research Associate, where he worked on single- and multicore double-clad and PCF lasers. Since 2005, he has been with Corning Inc., Corning, NY, as a Senior Research Scientist, working on the application of computational photonics to telecommunications and liquid crystal displays.

Axel Schülzgen received the Ph.D. degree in experimental physics from Humboldt-University Berlin, Berlin, Germany, in 1992.

From 1992 to 1995, he was a Research Fellow with Trinity College, Dublin, Ireland, and with Humboldt-University Berlin and studied the optical properties of low-dimensional semiconductor structures. In 1996, he joined the University of Arizona, Tucson, where he is currently working as a Research Professor at the College of Optical Sciences. His work focuses on the investigation of advanced micro- and nanostructured materials, novel nonlinear optical effects, ultrafast optics, and laser development.

Li Li, photograph and biography not available at the time of publication.

Valery L. Temyanko, photograph and biography not available at the time of publication.

Nasser Peyghambarian, photograph and biography not available at the time of publication.

Jerome V. Moloney, photograph and biography not available at the time of publication.